Supporting Information

Enantioselective Disruption of Cellulose Nanocrystals Self-Assembly into Chiral Nematic Phases in D-Alanine Solutions

David Attia [a], Orit Mendelson [b], Yael Levi-Kalisman [c], Ronit Bitton [a,d], Rachel Yerushalmi-Rozen [a,d,*]

[a] Department of Chemical Engineering, Ben-Gurion University of the Negev, Beer-Sheva 84105, Israel.

[b] Nuclear Research Center-Negev, Department of Chemistry, Beer-Sheva 84190, Israel.

[c] The Center for Nanoscience and Nanotechnology, The Institute of Life Sciences, The Hebrew University, Jerusalem 91904, Israel.

[d] The Ilse Katz Institute for Nanoscience and Technology, Ben-Gurion University of the Negev, Beer-Sheva 84105, Israel.

* Correspondence: rachely@bgu.ac.il

1. Materials and methods

1.1. Materials

Cellulose nanocrystals (CNCs). Sulfuric acid hydrolysed CNCs freeze-dried powder was purchased as a powder from Cellulose Lab Canada (CAS# 9004-34-6). The dimensions of the investigated CNCs, as reported by the manufacturer, are 5-20 nm width and 140-200 nm length. In water, these CNCs form an electrostatically stabilized suspension due to the sulfate half-ester groups on their surface with pKa ~ 1.99, [1] and electrokinetic potential of -38 ± 0.4 mV (in 0.38 mM sodium azide).

Amino acids. D-Alanine (CAS# 338-69-2), and L-Alanine (CAS# 56-41-7) powders were purchased from Acros Organics.

Sodium azide. The powder was purchased from Sigma Aldrich (CAS# 26628-22-8).

1.2. Preparation Methods

Preparation of CNCs suspensions. CNCs powder was suspended in Millipore water (18 MΩ·cm) by mixing for approximately 24 hours, followed by tip-sonication (130 W, 20 kHz, Ultrasonic processor model VCX-130, Sonics & Materials Inc., Newtown, CT, USA) at 30% amplitude for 4 minutes: The suspensions were tip-sonicated for 2 minutes, then vigorously hand-shaken, and tip sonicated for additional 2 minutes. The suspensions were cooled (in ice-water) during sonication to prevent the hydrolysis of the sulfate half-ester groups [2,3]. After the sonication, Sodium Azide was added to a final concentration of 0.38 mM (to prevent the growth of biological contaminations), the vials were sealed, and incubated in ambient conditions for two weeks.

Preparation of CNCs suspensions in amino acids solutions. Amino acid powders (D- or L-Alanine) were dissolved in pre-prepared CNCs suspension by mixing with a magnetic stirrer for 1-2 hours, and the vials were sealed and incubated in ambient conditions for two weeks.

1.3. Characterization

Electrokinetic Mobility. Mobility measurements of 0.1 wt% CNCs suspensions in water and in solutions of 0.2 wt% D- and L-Alanine were carried out using the Zetasizer Nano ZS (Malvern Instruments Ltd.). The measurements were performed at 25 ˚C and pH ~ 7.4 and repeated four times per sample. The Zeta potential of colloidal particles be calculated by using Henry's equation:

$$(S1)\ \zeta = \frac{3\mu_e \varepsilon_0 \varepsilon_r \eta}{2\ f(\kappa a)}$$

Where ζ is the calculated zeta potential, μ_e are the electrophoretic mobility, ε_r and ε_r is the relative dielectric constant and the dielectric constant in vacuum, respectively, η is the viscosity of the media, and $f(\kappa a)$ is the Henry's function (depends on the Debye length κ^{-1}). In a case of high dielectric constant and aqueous media, $f(\kappa a)$ equals to 1.5 and is referred to as the Smoluchowski approximation [4].

pH Measurements. pH measurements were carried out using Orion star a214 pH meter equipped with METER TOLEDO glass pH electrode, with ceramic junction ARGENTHAL™ Ag+-trap (Ag/AgCl) and 3 mol/L KCl reference electrolyte. The calibration of the pH meter was carried out by standard 4.01, 7, and 10.04 buffers.

Visual Inspection. The volume fraction of the nonisotropic phase ϕ_{LC} was determined by visual inspection of the samples in 4 mL glass vials. ϕ_{LC} was obtained by measuring the height of the nonisotropic phase and the height of the total volume of the suspension using ImageJ.

Polarized Optical Microscopy (POM). POM Images of CNC suspensions were taken using Olympus BX53-F2 microscope equipped with a high-resolution Olympus DP74 camera, in a crossed polarizers configuration and analyzed using ImageJ.

Small-Angle X-ray Scattering (SAXS). Scattering patterns of the solutions were collected using our in-house SAXSLAB GANESHA 300-XL Xenocs. CuKα radiation was generated by a Genix 3D Cu-source with an integrated monochromator. The scattering intensity *I(q)* was recorded using a two-dimensional Pilatus 300K detector in the interval of $0.007 < q < 0.25$ Å^{-1} (corresponding to the length scale of 25–900 Å), where the scattering vector is defined as $q = (4\pi/\lambda) \cdot \sin\theta$, with 2θ and λ being the scattering angle and wavelength, respectively. The long axis of the sample capillary is aligned in parallel to the z-axis of the 2D detector. The 2D SAXS patterns were azimuthally averaged using the two-dimensional data reduction SAXSGUI. This produced a one-dimensional scattering profile of the intensity, I, versus the scattering vector q. The measurements were performed under a vacuum at an ambient temperature. The solutions were sealed in thin-walled quartz capillaries about 1.5 mm in diameter and 0.01 mm wall thickness; The scattering curves were corrected for counting time and sample absorption. The scattering spectra of the solvent were subtracted from the corresponding solution data using the Irena package [5] in Igor Pro 9 from WaveMetrics (Portland, Oregon). The data analysis and model fitting were carried out using the SasView program, and Wolfram Mathematica software [6,7].

Circular Dichroism (CD). CD measurements were performed using J-715 spectropolarimeter (Jasco, Tokyo, Japan). The spectra were recorded in the range of 190-260 nm with 0.5 nm intervals in quartz cuvettes (optical path length of 0.1 cm).

CD spectroscopy [8,9] measures the difference in the absorption of left- and right-handed circularly polarized light (CPL), as it passes through a specimen:

$$(S2)\ \Delta A(\lambda) = A_L(\lambda) - A_R(\lambda)$$

Where $A_L(\lambda)$ and $A_R(\lambda)$ are the absorbed left- and right-circularly polarized light of the chiral object, respectively. At low concentrations, $\Delta A(\lambda)$ follows Beer-Lambert's law:

$$(S3)\ \Delta A(\lambda) = [\varepsilon_L(\lambda) - \varepsilon_R(\lambda)] \times l \times c_M$$

Where ε_L and ε_R are the molar absorption coefficient ($m^2 \cdot mol^{-1}$) or the left- and right-handed CPL, respectively, l represents the path length (cm), and c_M is the molar concentration ($mol \cdot L^{-1}$). $\Delta A(\lambda)$ is non-zero for a chiral object at a specific wavelength, and as a result, the CD spectrum can have either a positive or negative peak. The raw data obtained from CD measurements provide the change in ellipticity θ (milidegrees) with the wavelength λ, and can be expressed by:

$$(S4)\ \theta = 32.98 \cdot \Delta A(\lambda)$$

The measured ellipticity θ could be normalized and converted to molar ellipticity, as follow:

$$(S5)\ [\theta] = \frac{MW \times \theta}{10 \times l \times c}$$

Where $[\theta]$ is the molar ellipticity ($degree \cdot cm^2 \cdot dmol^{-1}$), MW is the molecular weight ($g \cdot mol^{-1}$), l is the path length (cm), and c is the concentration ($g \cdot L^{-1}$). This conversion to $[\theta]$ enables comparisons of CD spectra obtained from different samples independent of the specific conditions in which the data was collected (concentration, pathlength).

Cryogenic transmission electron microscopy (Cryo-TEM). Rapid cooling enables direct imaging of molecular assemblies and nanostructures in aqueous media. The samples were prepared by applying a 3 μL drop to a TEM grid (300 mesh Cu Lacey substrate, Ted Pella, Ltd., Redding, CA, USA) following a short pre-treatment of the grid via glow discharge. The excess liquid was blotted, and the specimen was vitrified by rapid plunging into liquid ethane precooled by liquid nitrogen using a vitrification robot system (Vitrobot Mark IV, FEI). The rapid cooling results in a physical fixation of the liquid state, so as to preserve the native assemblies, and prevents the formation of either cubic- or hexagonal ice. The vitrified samples were examined at -179 °C using FEI Tecnai 12 G^2 TWIN TEM operated at 120 kV and equipped with a Gatan model 626 cold stage. The images were recorded by a 4K×4K FEI Eagle CCD camera in low dose mode. TIA (Tecnai Imaging & Analysis) software was used to record the images.

Negative staining: To increase the inherently low contrast of the polymer assemblies, transmission electron microscopy imaging of dried, stained samples was performed. The solution (2 μL) was applied to a glow discharged TEM grid (carbon supported film on 300 mesh Cu grids, Ted Pella, Ltd., Redding, CA, USA). The excess liquid was blotted and the grids were washed on two droplets of de-ionized water

followed by staining with 2% Uranyl acetate for 40 s. The grids were blotted and dried under ambient conditions at room temperature before they were observed by FEI Tecnai 12 G^2 TWIN TEM operated at 120 kV. The images were recorded by a 4K×4K FEI Eagle CCD camera and using TIA (Tecnai Imaging & Analysis) software.

2. Macroscopic phase diagram

The macroscopic phase behavior of CNCs suspensions in 10 wt% Alanine solution is presented in Figure S1 and Table S1. In water (Figure S1A) the CNC suspensions undergo liquid-liquid crystalline (LC) phase separation at a critical concentration (c^*), where the upper phase is optically isotropic (I), and the lower phase is birefringent and cholesteric (chiral-nematic N^*). At the biphasic regime, the volume fraction of the LC phase (ϕ_{LC}) monotonically increases with CNCs' concentration up to a second critical concentration (c^{**}) where the suspension is fully nonisotropic [10,11]. In the solution of 10 wt% D-Alanine (Figure S1 B), the onset concentration of the biphasic I-N^* regime is delayed to a higher CNC concentration $c^* > 6$ wt%, as compared to $c^* > 4$ wt% in native CNCs suspension in water. Differently, in 10 wt% L-Alanine solutions the behavior is similar to Alanine-free suspensions (Figure S1 C, Table S3).

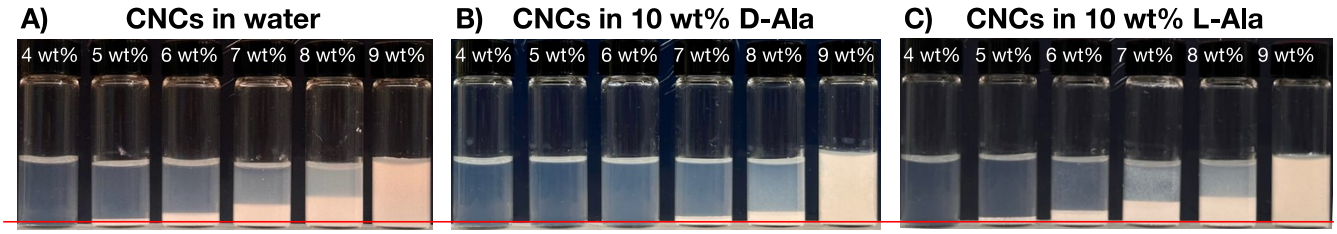

Figure S1. Images of CNCs suspensions in **A)** water, **B)** 10 wt% D-Alanine solutions **C)** 10 wt% L-Alanine solutions.

Table S1. The measured volume fraction of the nonisotropic phase ϕ_{LC} of CNCs suspensions in water, 10 wt% D-Alanine solutions, and 10 wt% L-Alanine solutions. 0.38 mM Sodium azide was added to all samples. The error is about 10% of the average measured value.

CNCs [wt%]	ϕ_{LC} in water [vol%]	ϕ_{LC} in 10 wt% D-Ala [vol%]	ϕ_{LC} in 10 wt% L-Ala [vol%]
4	0	0	0
5	8	0	7
6	18	0	18
7	35	12	34
8	49	25	50
9	100	100	100

3. Polarized Optical Microscopy (POM)

POM images of 5-8 wt% CNCs suspensions in water and 10 wt% Alanine solutions are presented in Figure S2 and Table S2. The POM images collected from the *N** phase exhibit the typical interference pattern characteristic of the *N** phase ("fingerprint pattern"). As previously reported [10], the helical pitch decreases with CNCs concentration, from $P = 22 \pm 3$ µm for 5 wt% to $P = 13 \pm 1$ µm for 8 wt%. Similarly, CNCs suspensions in 10 wt% L-Alanine show the same trend. However, 5 and 6 wt% CNCs suspensions in 10 wt% D-Alanine do not show the N* phase and are optically isotropic and thus appear black under the POM. These results are in agreement with the macroscopic phase diagram (Figure S1 B), where the *N** phase appears at $c^* > 6$ wt%. For 8 wt% CNCs, the pitch decreases from $P = 13 \pm 1$ µm in water to $P = 10 \pm 1$ µm in 10 wt% D-Alanine

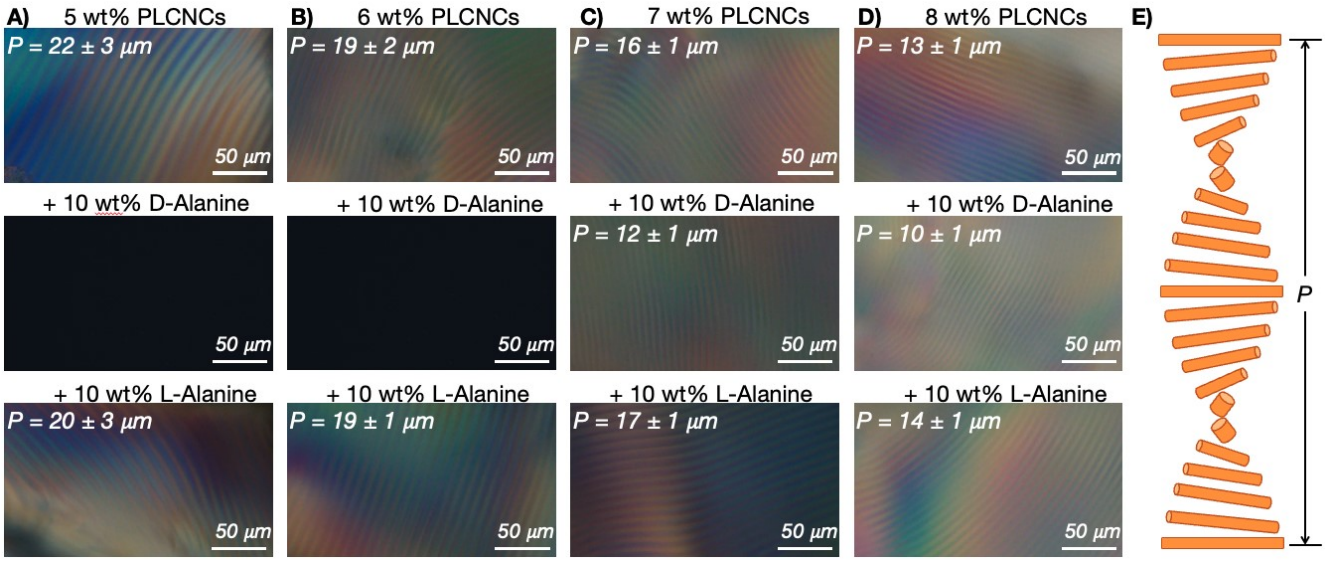

Figure S2. POM images of **A)** 5, **B)** 6, **C)** 7, and **D)** 8 wt% CNCs in water, 10 wt% D- and L-Alanine. **E)** Schematics presenting the helical modulation of the N* phase pitch, defined as the length in which the director fulfills a full rotation (the unit vector is coupled to the long axis of the rod). The distance between two adjacent elongation lines is the half pitch.

Table S2. Characteristic pitch values of the LC phase of PLCNCs suspensions in water, 10 wt% D-Alanine solutions, and 10 wt% L-Alanine solutions.

CNCs [wt%]	*N** phase Pitch [µm]		
	Water	10 wt% D-Ala	10 wt% L-Ala
5	22 ± 3	There is no *N**	20 ± 3
6	19 ± 2	There is no *N**	19 ± 1
7	16 ± 1	12 ± 1	17 ± 1
8	13 ± 1	10 ± 1	14 ± 1

4. Small-Angle X-ray Scattering (SAXS) measurements of the N* phase

The nanostructure of CNCs suspensions in solutions of 10 wt% D- and L-Alanine were investigated using SAXS and compared with CNCs suspensions in water. 1-7 wt% CNCs suspensions were prepared and incubated in ambient conditions for approximately two weeks. Then, spontaneous phase separation was observed in a concentration range of 4 to 7 wt% CNCs, and SAXS measurements of both the upper and lower phases were carried out. Figure S3 A presents 2D scattering patterns obtained from 1-7 wt% CNCs suspensions in water. Below 5 wt%, only isotropic 2D patterns are observed, in accordance with the macroscopic phase diagram (Figure S1-A). The corresponding 1D pattern obtained from 1 wt% CNCs suspension (Figure S3 B) exhibits a typical form factor of parallelepipeds particles (see Figure S7). At CNC concentrations > 5 wt%, the 2D patterns, collected from the lower phase are nonisotropic. The corresponding 1D scattering presented in Figure S3 B shows a structure factor above 2 wt% CNCs. Below c^*, the appearance of the structure factor indicates the presence of the microscopically nematically ordered islands, known as tactoids [12,13]. The 1D peak at low q-values (q_0) and a shoulder, q_1, at the mid-high q regime are clearly observed. The primary peak, q_0, can be used to calculate the interparticle distance d_0 via Bragg's law, $d_0 = 2\pi/q_0$. The ratio of the two peaks, q_1/q_0, corresponds to 2:1, implying a lamellar symmetry [14]. The values of the peak and shoulder were determined by a fit of a Gaussian function (Equation S4) to the Lorentz-corrected intensities plot, which is a plot of the change in $I(q)\cdot q^2$ versus q (Figure S3 C):

$$(S4)\ I(q) = A\exp\left\{-(q-q_0)/w^2\right\} + background$$

Where *background* and A are constants, q_0 is the average q-value corresponding to the relevant peak (q_0 or q_1), and w is the distribution width. The calculated values of the different parameters are summarized in Table S3.

Above 1 wt% CNCs, the scattering curves were fitted to the parallelepiped stacking model developed by Mao *et al.* [7,15]. In this model, due to cellulose crystalline structure and unit cell, the individual CNC particle is modeled as rectangular shaped parallelepiped of width a, thickness b, and length L. These parallelepipeds are stacked in a preferred direction, and the average distance between two adjacent particles is abbreviated as the interparticle distance, d_0. The best-fitting parameters are presented in Table S3. As previously reported by us and others [16–18], the position of the primary peak shifts to higher q-values with the increase in CNCs' concentration, as the interparticle distance decreases (Table S3). However, the average a and b values are not modified by the CNCs concentration.

Figures S3 D-E show 2D SAXS patterns and the corresponding 1D curves of the upper and lower phases of the CNCs suspensions. While the upper phases exhibit isotropic 2D patterns, the lower phases are

nonisotropic. Both the primary and secondary peaks of the upper phase are smeared and broader than those of the lower phase. As a result, the error in the calculated values of the interparticle distance, $d_{0,}$ is larger.

SAXS of CNCs suspensions in solutions of 10 wt% L-Alanine present similar scattering patterns to the Alanine-free suspensions: the shape of the curves, location of the peaks, and the value of the best-fitted parameters (Figure S4 and Table S3) are similar. However, in solutions of 10 wt% D-Alanine, several major differences can be detected (Figure S5 and Table S3). First, the structure factor is only observed at CNCs concentrations above 4 wt% CNCs (as compared to 2 wt% for CNCs suspensions in Alanine-free (or L-Alanine) suspensions. Second, the 2D patterns are fully isotropic up to 7 wt% (in agreement with the macroscopic phase diagram, Figure S1 C). Moreover, the scattering patterns obtained from these suspensions (5 wt% in D-Alanine) are different from the SAXS curves that were collected from both the isotropic (upper) and nematic (lower) phase of 5 wt% CNCs in water (main text, Figure 3D). Thus, we conclude that the chiral environment in D-Alanine solutions affects the self-assembly of CNCs.

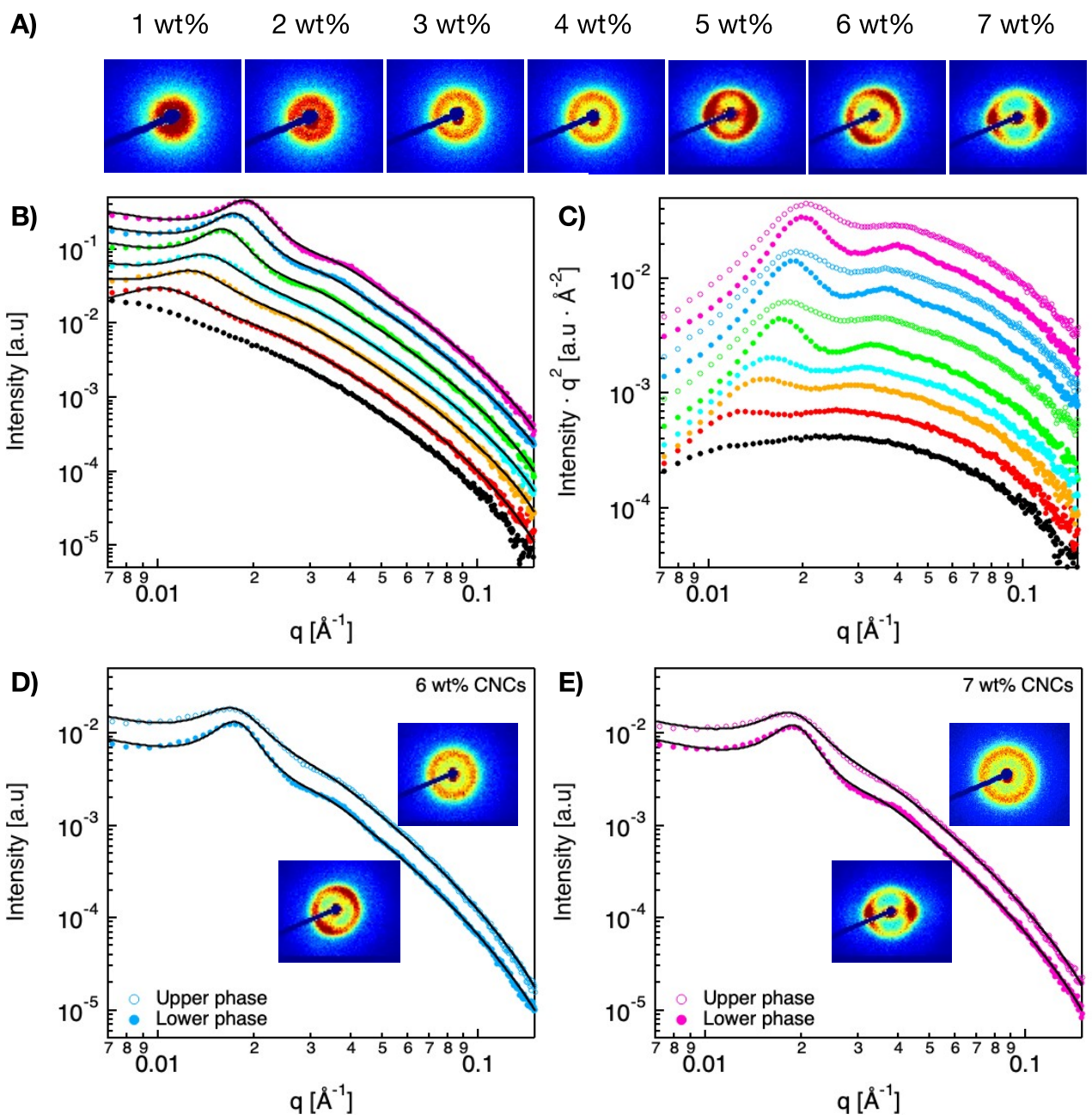

Figure S3. A) 2D SAXS patterns, **B)** background-subtracted 1D scattering curves, and **C)** Lorentz-corrected intensities ($I(q)\cdot q^2$) of 1-7 wt% CNCs suspensions in water. Color code: 1 wt% ᔓ, 2 wt% ᔓ, 3 wt% ᔓ, 4 wt% ᔓ, 5 wt% ᔓ, 6 wt% ᔓ, 7 wt% ᔓ. Comparison between the upper and lower phases of **D)** 6 wt%, and **E)** 7 wt% CNCs in water (0.38 mM sodium azide). The solid lines represent a fit to the parallelepiped stacking model [15]. The curves are shifted for better visualization. Upper phase: ◯, lower phase: ᔓ.

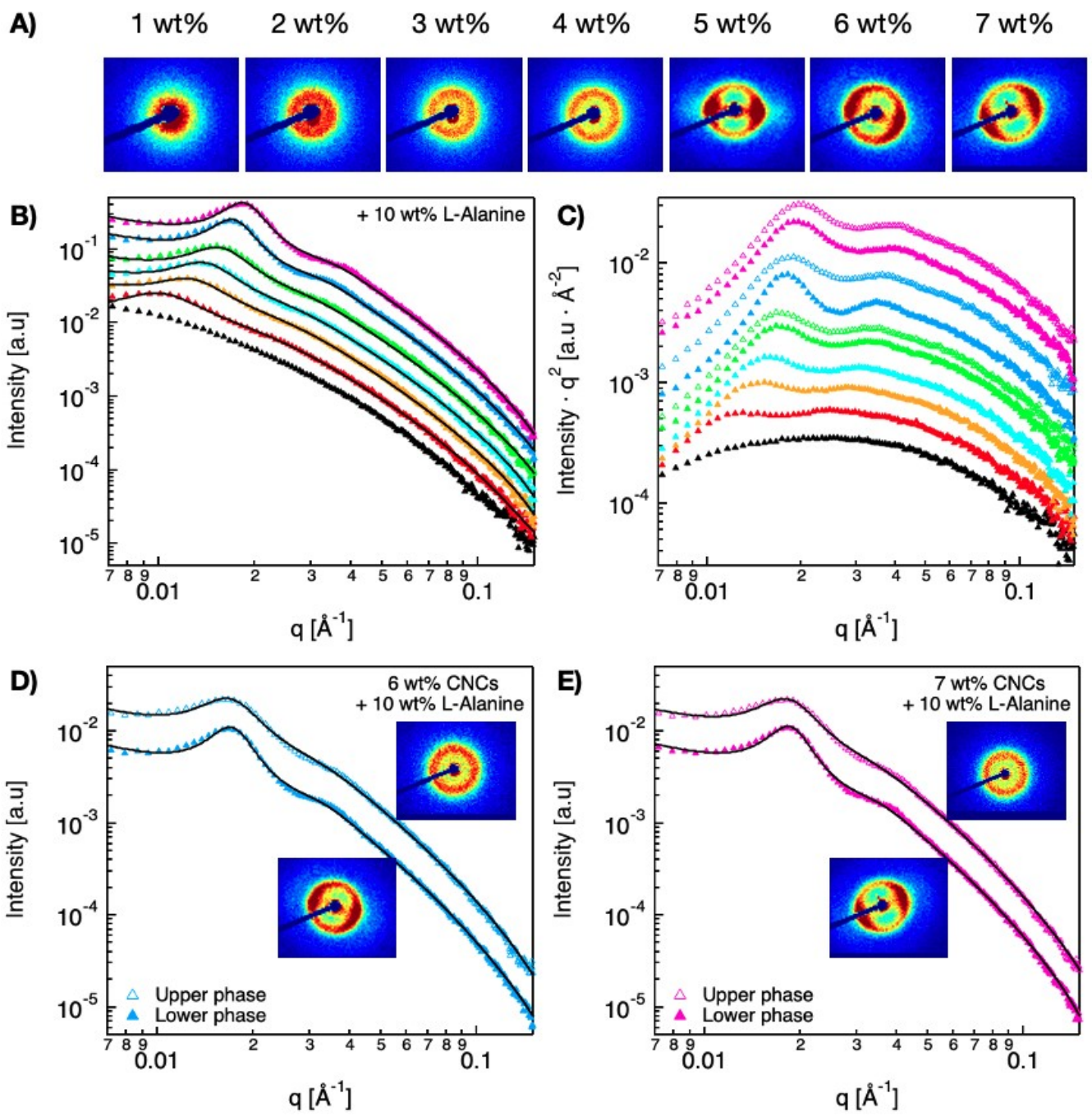

Figure S4. A) 2D SAXS patterns, **B)** background-subtracted 1D scattering curves and **C)** Lorentz-corrected intensities $I(q)\cdot q^2$ of 1-7 wt% CNCs suspensions in 10 wt% L-Alanine solutions. Color code: 1 wt% ▲, 2 wt% ▲, 3 wt% ▲, 4 wt% ▲, 5 wt% ▲, 6 wt% ▲, 7 wt% ▲.Comparison between the upper and lower phases of **D)** 6 wt%, and **E)** 7 wt% CNCs in 10 wt% L-Alanine solutions (0.38 mM sodium azide). The solid lines represent a fit to the parallelepiped stacking model [15]. The curves are shifted for better visualization. Upper phase: △, lower phase: ▲.

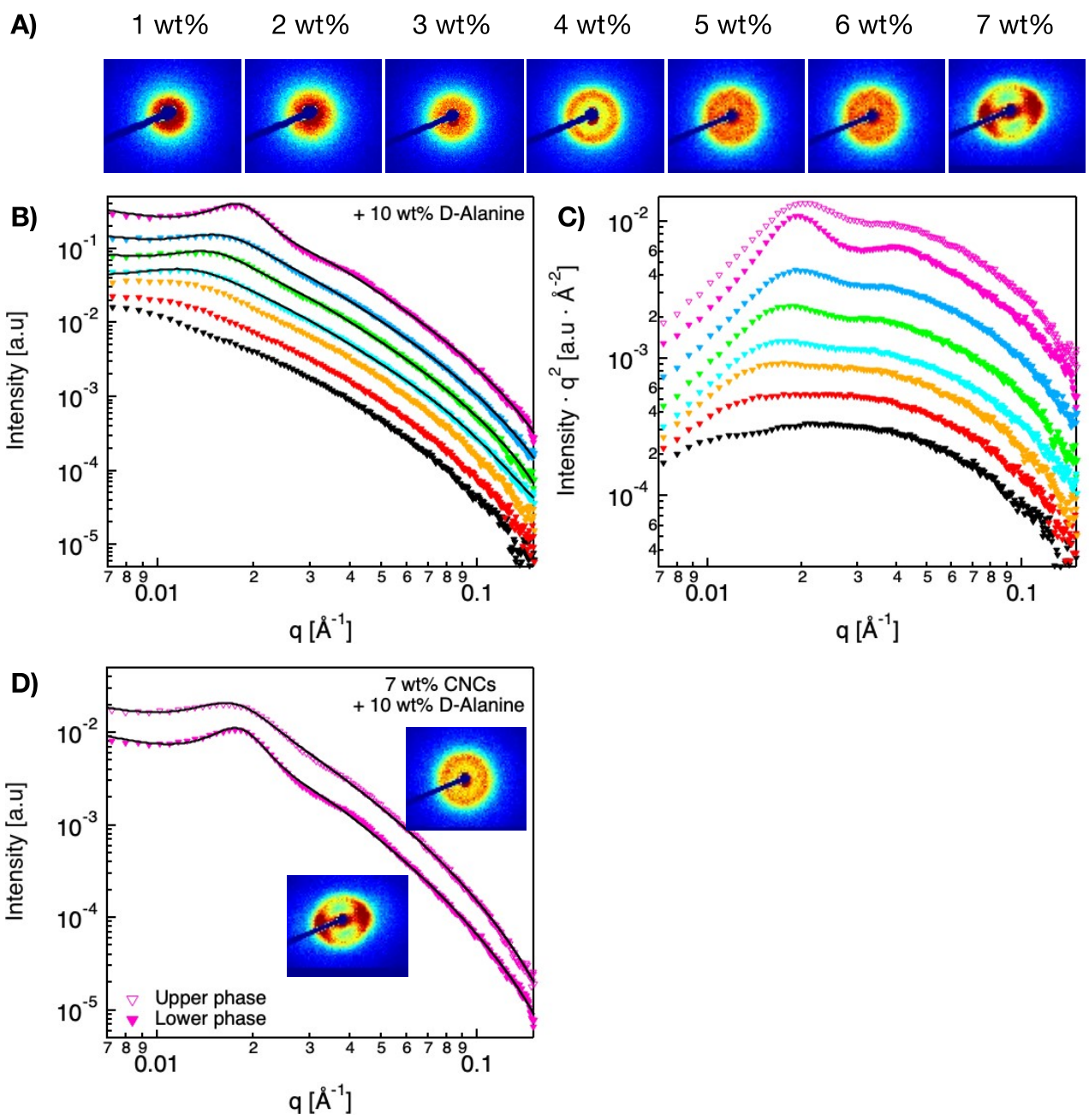

Figure S5. A) 2D SAXS patterns, **B)** background-subtracted 1D scattering curves, and **C)** Lorentz-corrected intensities $I(q)\cdot q^2$ of 1-7 wt% CNCs suspensions in 10 wt% D-Alanine solutions (0.38 mM sodium azide). Color code: 1 wt% ▼, 2 wt% ▼, 3 wt% ▼, 4 wt% ▼, 5 wt% ▼, 6 wt% ▼, 7 wt% ▼. Comparison between the upper and lower phases of **D)** 7 wt% CNCs in 10 wt% D-Alanine solutions. The solid lines represent a fit to the parallelepiped stacking model [15]. The curves are shifted for better visualization. Upper phase: ▽, lower phase: ▼.

Table S3. SAXS data of 2-7 wt% CNCs suspensions in water. The typical thickness $\langle a \rangle$, width $\langle b \rangle$, and the inter-plate distance $\langle d_0 \rangle$ as determined from the parallelepiped stacking model [15]. The values of the scattering vectors, which correspond to the primary and secondary peaks in the Lorentz-corrected intensities plot, q_0 and q_1, respectively, were estimated by fitting a Gaussian function to the relevant peak.

Solvent	*CNCs* [wt%]	Phase	q_0 [Å^{-1}]	q_1 [Å^{-1}]	q_1/q_0	$\langle a \rangle$ [nm] ± 1	$\langle b \rangle$ [nm] ± 2	$\langle d_0 \rangle$ [nm]
Water	2	*I*	0.0136	0.0260	1.91 :1	3	14	57 ± 20
	3	*I*	0.0153	0.0292	1.91 :1	2	14	45 ± 14
	4	*I*	0.0165	0.0314	1.90 :1	2	14	41 ± 13
	5	*I*	0.0180	0.0340	1.89 :1	2	14	36 ± 11
		*N**	0.0172	0.0332	1.93 :1	2	16	36 ± 9
	6	*I*	0.0193	0.0366	1.90 :1	2	13	33 ± 10
		*N**	0.0187	0.0360	1.93 :1	2	15	33 ± 9
	7	*I*	0.0209	0.0378	1.81 :1	2	13	33 ± 9
		*N**	0.0202	0.0397	1.97 :1	2	14	30 ± 8
10 wt% D-Alanine	4	*I*	0.0178	0.032	1.80 :1	3	16	45 ± 19
	5	*I*	0.0185	0.033	1.78 :1	2	14	39 ± 14
	6	*I*	0.0199	0.0366	1.84 :1	3	14	35 ± 13
	7	*I*	0.0206	0.0377	1.83 :1	3	14	32 ± 12
		*N**	0.0196	0.0388	1.98 :1	2	15	31 ± 9
10 wt% L-Alanine	2	*I*	0.0133	0.0254	1.91 :1	3	14	58 ± 20
	3	*I*	0.0152	0.0289	1.90 :1	2	14	46 ± 15
	4	*I*	0.0160	0.0308	1.93 :1	2	14	42 ± 13
	5	*I*	0.0173	0.0332	1.92 :1	2	13	37 ± 11
		*N**	0.0174	0.0333	1.91 :1	2	13	37 ± 11
	6	*I*	0.0187	0.0336	1.80 :1	2	13	34 ± 10
		*N**	0.0181	0.0354	1.96 :1	2	14	34 ± 8
	7	*I*	0.0203	0.0385	1.90 :1	2	12	31 ± 9
		*N**	0.0196	0.0388	1.98 :1	2	13	31 ± 8

5. Molecular interaction between D-Alanine and individual CNCs rods

The origins and mechanism leading to chiral discrimination in CNCs self-assembly in D-Alanine solutions could have resulted from condensation or adsorption of D-Alanine molecules onto the surface of CNCs.

In such a scenario, one would expect depletion of free alanine from the solution, leading to a reduction in the measured signal (ellipticity) in circular dichroism (CD) measurements as compared to Alanine solutions of similar concentrations.[19,20] Figure 2 of the main text demonstrates that the presence of CNCs does not modify the spectra measured in solutions of Alanine. Here we present complementary measurements of the CD signal obtained from CNC solutions at different concentrations (Figure S6 A). The CD spectra of CNC suspensions (concentrations of 0.1, 0.2, and 0.3 wt%) do not show a peak. In Figure S6 B, we present the effect of 0.2 wt% CNCs on the CD signal obtained from 2 concentrations of either D- or L-Alanine. In this experiment, we would expect that adsorption (or condensation) of Alanine onto the CNCs would lead to the depletion of Alanine from the solution, and thus the CD signal would be reduced [19]. Such an effect is not observed, and the spectra are not affected by the presence of the CNCs.

In addition, we carried out a complementary experiment, presented in Figure S6 C: The CD signal from a racemic solution of D and L-Alanine (0.04 wt% D-Alanine + 0.04 wt% L-Alanine) was measured in the absence and presence of 0.2 wt% of CNCs (Figure S6 C). Enantio-selective adsorption of Alanine onto the CNCs would lead to depletion of the preferred enantiomer from the solution, and thus, the balance between the enantiomers would be disrupted, and a peak of the non-adsorbed enantiomer should have appeared. However, no effect of CNCs on the CD signal of the racemic solution could be detected, suggesting that enantio-selective adsorption or condensation does not take place.

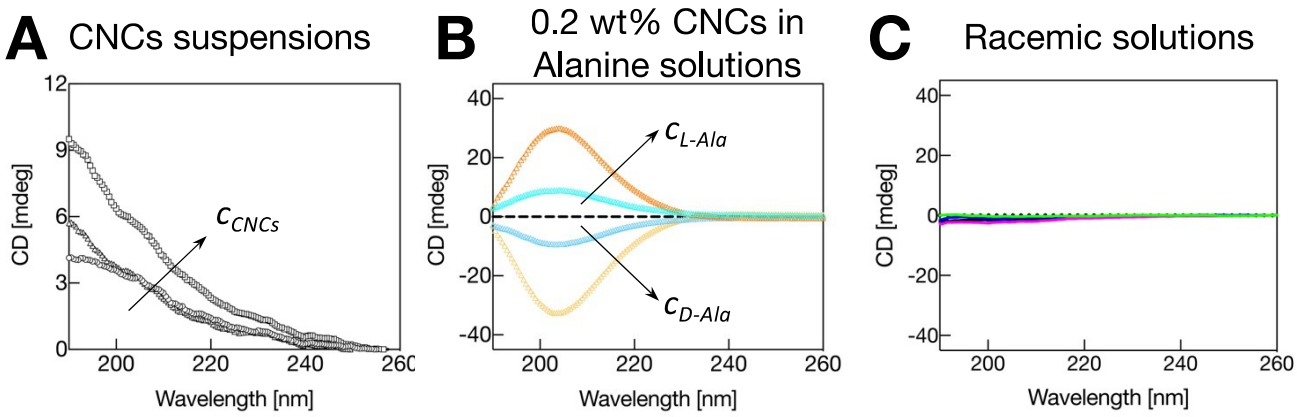

Figure S6. Circular Dichroism (CD) spectra of **A)** 0.1 ○, 0.2 △, and 0.3 wt% □ CNCs suspensions. **B)** D- and L-Alanine solutions in the presence of 0.2 wt% CNCs (hollow symbols). Alanine concentrations: 0.04 wt% ●, and 0.16 wt% ●. The spectra of the solvent (0.38 mM sodium azide solution) and 0.2 wt% CNCs were subtracted. **C)** CD spectra of racemic solutions (total concentration of 0.08 wt% Alanine) in water (black), 0.1 (magenta), 0.2 (blue), and 0.3 wt% (green) CNCs.

6. SAXS measurements of dilute and semi-dilute suspensions of CNCs: the Individual particle

SAXS measurements of CNCS suspensions in concentrations of 1, 1.5, and 2 wt% CNCs were carried out. The 1D SAXS profiles presented in Figure S8 could be fitted to the parallelepiped model [21] under

the assumption that the interactions between CNCs particles can be neglected due to the low CNC concentration and, thus, the structure factor *S(q) = 1*. The model is given by the equations:

$$(S1)\ I(q) = constant \cdot V \cdot (\rho_P - \rho_s)^2 \cdot \langle P(q,\alpha,\beta) \rangle$$

$$(S2)\ P(q,\alpha,\varphi) = \frac{1}{(abL)^2} \cdot \frac{1}{\pi} \int_0^{\pi} \int_0^{\pi/2} \left(\frac{2\sin\left[q\frac{L}{2}\cos\alpha\right]}{q\cos\alpha} \cdot \frac{4\sin\left[q\frac{a}{2}\sin\alpha \cdot \sin\varphi\right] \cdot \sin\left[q\frac{b}{2}\sin\alpha \cdot \cos\varphi\right]}{q^2\sin^2\alpha \cdot \sin\varphi \cdot \cos\varphi} \right)^2 \sin\alpha d\alpha d\varphi$$

Where V is the volume of the parallelepiped, ρ_p and ρ_s are the scattering length of the particles and solvent, respectively. The parallelepiped dimensions are defined as the thickness a, the width b, and the length L, which obey the criteria $a \leq b \leq L$. *P(q, α, φ)* is the parallelepiped form factor, at an angle *α* (the angle between the long axis in the direction of L and the scattering vector. *φ* is the angle between the projection of the particle in the xy-detector plane and the y-axis.

The CNC length was fixed to 140 nm, as previously estimated by cryo-TEM measurements [18]. The best-fitting parameters correspond to CNCs particles, with an average cross-section of (4.4 ± 0.2) × (13.8 ± 0.3) nm^2. The SAXS profiles obtained from CNCs suspension in 10 wt% D- or L-Alanine are similar to the Alanine-free suspension, (Table S5). All curves exhibit a q^{-1} slope at low *q*-regime (0.015 Å^{-1} < *q* < 0.025 Å^{-1}), typical for individual elongated rods, where a, b << L, and q^{-4} at the high *q*-region (0.075 Å^{-1} < *q* < 0.100 Å^{-1}) characteristic of a sharp cross-section and smooth interface [22] (Table S5). Thus, SAXS profiles do not provide any indication for adsorption or condensation of Alanine onto the CNCs.

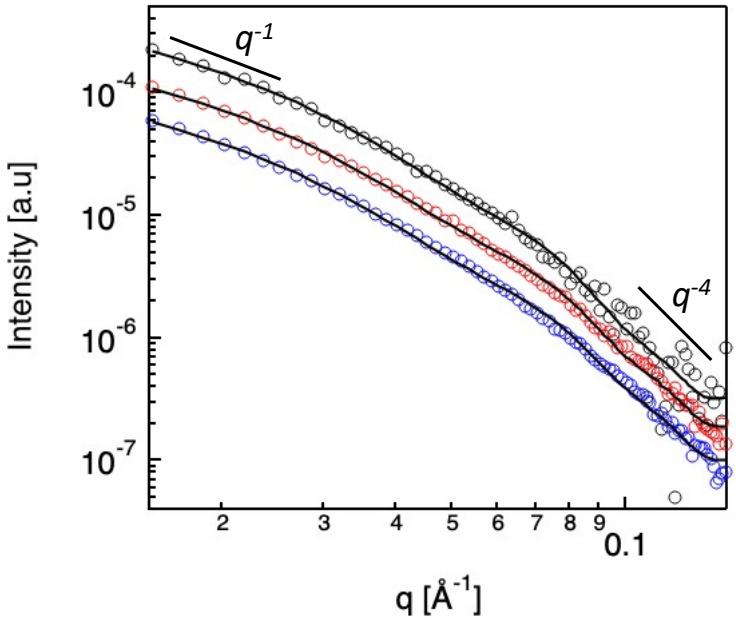

Figure S7. 1D background-subtracted curves obtained from dilute suspensions of 0.1 wt% CNCs in water ○, in 10 wt% L-Alanine ○, and 10 wt% D-Alanine ○. The solid black lines are fitting to a parallelepiped form-factor [21]. The curves are shifted for better visualization.

Table S4. The best-fitting parameters to the parallelepiped model [21], where a is the thickness and b is the width. A power law could be fitted to low and high q-regions of the scattering curves of CNCs in water, 10 wt% D- and L-Alanine.

Sample	$\langle a \rangle$ [nm]	$\langle b \rangle$ [nm]	Power Low q-region (Guinier)	Power High q-region (Porod)
0.1 wt% CNCs	4.4 ± 0.2	13.8 ± 0.3	-0.9 ± 0.3	-3.7 ± 0.4
+ 10 wt% L-Alanine	4.5 ± 0.1	13.5 ± 0.1	-0.9 ± 0.1	-3.8 ± 0.4
+ 10 wt% D-Alanine	4.4 ± 0.1	13.6 ± 0.1	-1.2 ± 0.1	-3.8 ± 0.3

Figure S9 presents the scattering patterns obtained from deionized water (DIW) and 10 wt% D-Alanine solution. As can be observed, the scattering from 10 wt% D-Alanine solutions is similar to that of water.

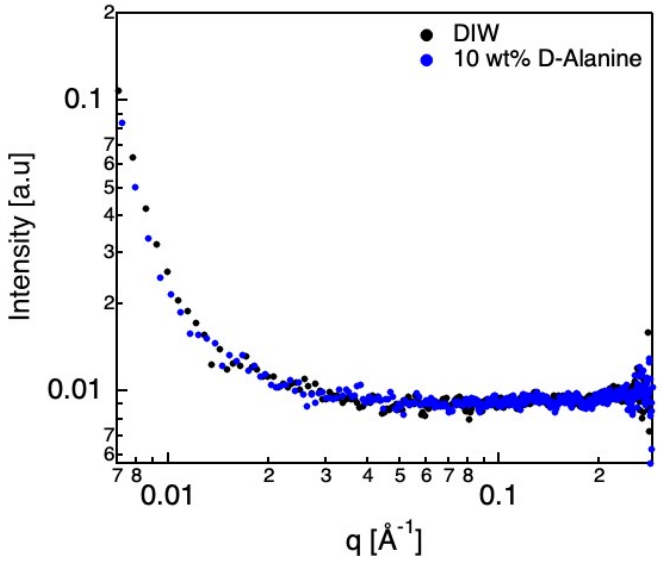

Figure S8. 1D SAXS from deionized water (DIW) ꝏ, and 10 wt% D-Alanine aqueous solution ꝏ.

7. Zeta potential and pH measurements

The measured values of electrokinetic mobility of 0.1 wt% CNCs suspensions in water, 0.2 wt% D- and L-Alanine solutions are similar (Tables S6). The measured pH values of 0.1 wt% CNCs suspensions in water and in 0.2 wt% D- and L-Alanine are 7.3 ± 0.1, and of 7 wt% CNCs in water and in 10 wt% D- and L-Alanine are 6.4 ± 1.

Table S5. Measured mobility and the calculated Zeta potential of 0.1 wt% CNCs in aqueous suspensions containing 0.38 mM sodium azide and solutions of D or L Alanine (0.2 wt%).

Sample	Mobility [μm·cm·V^{-1}·s^{-1}]	Zeta potential [mV]
0.1 wt% PLCNCs	-2.96 ± 0.03	-37.8 ± 0.4
+ 0.2 wt% D-Alanine	-3.00 ± 0.10	-38.3 ± 1.4
+ 0.2 wt% L-Alanine	-2.68 ± 0.02	-34.3 ± 0.3

8. CNCs self-assembly in sodium azide-free suspensions

In the experiment presented in Figure S9, 6 wt% CNCs suspensions were titrated with D-Alanine solution at concentrations of 1 to 10 wt%. The results indicate that there exists a threshold concentration of D-Alanine for modifying the phase diagram of CNCs: the volume fraction of the *N** phase, in 6 wt% CNCs suspensions, reduces with increasing concentration of D-Alanine, and almost fully disappears in solutions of 10 wt% D-Alanine (Figure S9 A,B). The *pitch* of the residual *N** (Figure S9 C) reduces from $P = 19 \pm 2$ μm in water to $P = 14$ μm ± 1 μm in D-Alanine solutions and is hardly affected by the overall concentration of D-Alanine.

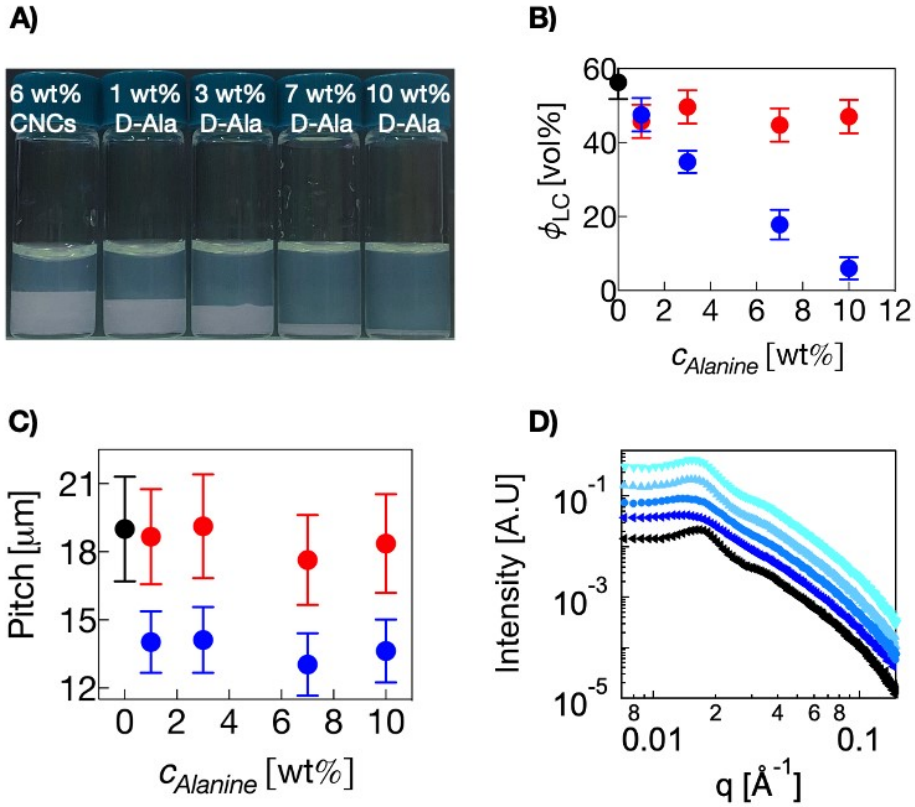

Figure S9. A) Optical image taken between two crossed polarizers of 6 wt% CNCs in 1-10 wt% D-Alanine. **B)** Volume fraction of the *N** phase as a function of Alanine concentration. **C)** Pitch as a function of CNCs concentration in water ꩜, L-Alanine concentration ꩜, and

D-Alanine concentration ∞. **D)** 1D SAXS patterns of 6 wt% CNCs in water ◀□, 1 wt% ▼, 3 wt% ▲, 7 wt% ∞, and 10 wt% D-Alanine ◀□. All the suspensions are sodium azide-free. The curves are shifted for better visualization.

References

1 S. Elazzouzi-Hafraoui, Y. Nishiyama, J. L. Putaux, L. Heux, F. Dubreuil and C. Rochas, *Biomacromolecules*, DOI:10.1021/bm700769p.
2 P. Lu and Y. Lo Hsieh, *Carbohydr Polym*, DOI:10.1016/j.carbpol.2010.04.073.
3 D. Klemm, F. Kramer, S. Moritz, T. Lindström, M. Ankerfors, D. Gray and A. Dorris, *Angewandte Chemie - International Edition*, 2011, 50.
4 J. W. Swan and E. M. Furst, *J Colloid Interface Sci*, DOI:10.1016/j.jcis.2012.08.026.
5 J. Ilavsky and P. R. Jemian, *J Appl Crystallogr*, DOI:10.1107/S0021889809002222.
6 L. Tan, J. G. Elkins, B. H. Davison, E. G. Kelley and J. Nickels, *J Appl Crystallogr*, DOI:10.1107/S1600576720015526.
7 Y. Mao, K. Liu, C. Zhan, L. Geng, B. Chu and B. S. Hsiao, *Journal of Physical Chemistry B*, DOI:10.1021/acs.jpcb.6b11425.
8 B. Ann. Wallace and R. William. Janes, *Modern techniques for circular dichroism and synchrotron radiation circular dichroism spectroscopy*, IOS Press, Amsterdam, 2009.
9 D. S. Rodgers, *Circular dichroism theory and spectroscopy*, Nova Science Publishers, New York, 2012.
10 Y. Habibi, L. A. Lucia and O. J. Rojas, *Chem Rev*, DOI:10.1021/cr900339w.
11 J. P. F. Lagerwall, C. Schütz, M. Salajkova, J. Noh, J. H. Park, G. Scalia and L. Bergström, *NPG Asia Mater*, 2014, 6.
12 P. X. Wang, W. Y. Hamad and M. J. MacLachlan, *Nat Commun*, DOI:10.1038/ncomms11515.
13 Q. Sun, V. Lutz-Bueno, J. Zhou, Y. Yuan and P. Fischer, *Nanoscale Adv*, DOI:10.1039/d2na00303a.
14 P. Alexandridis, U. Olsson and B. Lindman, *Langmuir*, DOI:10.1021/la971117c.
15 Y. Mao, M. Bleuel, Y. Lyu, X. Zhang, D. Henderson, H. Wang and R. M. Briber, *Langmuir*, DOI:10.1021/acs.langmuir.8b01452.
16 C. Schütz, M. Agthe, A. B. Fall, K. Gordeyeva, V. Guccini, M. Salajková, T. S. Plivelic, J. P. F. Lagerwall, G. Salazar-Alvarez and L. Bergström, *Langmuir*, DOI:10.1021/acs.langmuir.5b00924.
17 N. Cohen, D. Attia, Y. Levi-Kalisman, R. Bitton and R. Yerushalmi-Rozen, *Polym Adv Technol*, DOI:10.1002/pat.5647.
18 D. Attia, N. Cohen, G. Ochbaum, Y. Levi-Kalisman, R. Bitton and R. Yerushalmi-Rozen, *Soft Matter*, DOI:10.1039/d0sm01025a.
19 L. Lugasi, G. Otis, M. Oliel, S. Margel and Y. Mastai, *Polym Adv Technol*, DOI:10.1002/pat.5667.
20 P. Paik, A. Gedanken and Y. Mastai, *ACS Appl Mater Interfaces*, DOI:10.1021/am9003842.
21 R. Nayuk and K. Huber, *Zeitschrift fur Physikalische Chemie*, DOI:10.1524/zpch.2012.0257.
22 R.-J. Roe, *Methods of X-ray and neutron scattering in polymer science*, 2000.